NASA TECHNICAL MEMORANDUM

NASA TM X-52816

NASA TM X-52816

EXTERNALLY PRESSURIZED GAS-LUBRICATED JOURNAL BEARINGS WITH HERRINGBONE GROOVES - LOAD CAPACITY AND STABILITY ANALYSIS

by David P. Fleming
Lewis Research Center
Cleveland, Ohio

TECHNICAL PAPER proposed for presentation at Lubrication Conference sponsored by the American Society of Lubrication Engineers and the American Society of Mechanical Engineers
Cincinnati, Ohio, October 13-15, 1970

COVER Page NOT CORRECT

NASA TECHNICAL MEMORANDUM

NASA TM X-52816

NASA TM X-52816

EXTERNALLY PRESSURIZED GAS-LUBRICATED JOURNAL BEARINGS WITH HERRINGBONE GROOVES - LOAD CAPACITY AND STABILITY ANALYSIS

by David P. Fleming
Lewis Research Center
Cleveland, Ohio

TECHNICAL PAPER proposed for presentation at
Conference on Externally Pressurized Bearings sponsored by the
Institution of Mechanical Engineers and the Institution
of Production Engineers
Coventry, England, April 14-15, 1971

EXTERNALLY PRESSURIZED GAS-LUBRICATED JOURNAL BEARINGS WITH HERRINGBONE GROOVES - LOAD CAPACITY AND STABILITY ANALYSIS

by David P. Fleming

Lewis Research Center
Cleveland, Ohio

TECHNICAL PAPER proposed for presentation at

Lubrication Conference
sponsored by the American Society of Lubrication Engineers
and the American Society of Mechanical Engineers
Cincinnati, Ohio, October 13-15, 1970

NATIONAL AERONAUTICS AND SPACE ADMINISTRATION

EXTERNALLY PRESSURIZED GAS-LUBRICATED JOURNAL BEARINGS WITH HERRINGBONE GROOVES - LOAD CAPACITY AND STABILITY ANALYSIS

by David P. Fleming

Lewis Research Center
National Aeronautics and Space Administration
Cleveland, Ohio

ABSTRACT

A small eccentricity analysis was performed to predict load capacity and stability. Numerical results were obtained for a range of feeding parameter, pressure ratio, groove length and orifice recess volume for compressibility numbers from 0 to 50. These results were obtained from a digital computer program. Results showed that the addition of herringbone grooving to an externally pressurized bearing increases stability, but reduces load capacity at low compressibility numbers. A fully-grooved bearing is more stable than a partially-grooved bearing. Orifice recesses reduce stability, especially at high compressibility numbers.

NOMENCLATURE

a orifice radius

C ridge clearance at zero eccentricity

$\mathcal{C}$ coefficient (see appendix)

D bearing diameter

d orifice recess diameter

e journal eccentricity

F bearing load component

f	dimensionless load component, $F/\epsilon p_a LD$
G	dimensionless complex function of ζ
H	ratio of ridge clearance to groove clearance when bearing is concentric, $\left(h_g/h_r\right)_o$
h_g	local film thickness over groove, $C(H + \epsilon \cos \theta^*)$
h_r	local film thickness over ridge, $C(1 + \epsilon \cos \theta^*)$
$\mathfrak{Im}$	imaginary part of experssion
i	$\sqrt{-1}$
k	specific heat ratio
L	bearing length
L_f	length of bearing outboard of orifices
L_g	total axial length of grooves
M	rotor mass per bearing
$\dot{m}$	lubricant flow rate per unit length
$\overline{M}$	dimensionless rotor mass, $\left(Mp_a/2L\mu^2\right)(C/R)^5$
m	dimensionless lubricant flow rate, eq. (12)
N	number of orifices per bearing
P	dimensionless pressure, p/p_a
p	pressure
p_a	atmospheric pressure
R	bearing radius
$\mathfrak{R}$	gas constant
$\mathfrak{Re}$	real part of expression
T	absolute temperature
t	time

U_g surface speed of grooved member

U_p surface speed of smooth number

V orifice recess volume

v orifice recess volume, $NV/\pi DLC$

W total bearing load

$\overline{W}$ dimensionless load, $W/\epsilon p_a LD$

z axial coordinate measured from end of bearing

α ratio of groove width to width of groove-ridge pair

α_d orifice discharge coefficient

β groove angle (fig. 1)

δ inherent compensation factor, a^2/dC

ϵ eccentricity ratio, e/C

ζ dimensionless axial coordinate, z/L

ζ_f $L_f/2L$

ζ_g $L_g/2L$

θ angular coordinate

θ^* rotating angular coordinate, $\theta - \omega_p t$

Λ bearing compressibility number, $6\mu\omega R^2/p_a C^2$

Λ_s $6\mu L(U_p - U_g)/p_a C^2$

Λ_t feeding parameter, $6\mu N a^2 \sqrt{\mathcal{R}T}/p_a C^3 \sqrt{1 + \delta^2}$

μ lubricant dynamic viscosity

ρ local lubricant density

σ frequency number, $12\mu\omega_p R^2/p_a C^2$

φ attitude angle

ψ_0 $-(\Lambda_t/2P_{0c})\left[\partial m/\partial(P_c/P_s)\right]\Big|_{\epsilon=0}$

ψ_1 $NV/\pi D^2 C P_{0c}$

ω rotational speed

ω_p whirl frequency

Subscripts:

c condition immediately downstream of orifice

g groove region

n condition at which $f_t = 0$

r radial; ridge region

s condition upstream of orifice

t tangential

z axial direction

θ circumferential direction

0 zero eccentricity

Superscripts:

$^+$ value of coordinate infinitesimally greater than base value

$^-$ value of coordinate infinitesimally less than base value

INTRODUCTION

Gas-lubricated bearings may be divided into two broad classifications: self-acting and externally pressurized. In a self-acting bearing, the film pressure which supports the load is developed by the relative motion of the bearing parts and is proportional to the fluid viscosity. When there is no motion, the load capacity is zero. In contrast, in an externally pressurized bearing, lubricant gas under pressure is supplied from an external source. Thus, this type of bearing can have a substantial load capacity even when stationary.

Because of the low viscosity of gases, self-acting gas-lubricated bearings will carry a much smaller load than oil-lubricated bearings. For the same reason, they are much more susceptible to self-excited instability, commonly known as fractional frequency whirl. A major part of the research in gas-lubricated bearings has been directed toward development of bearing configurations that will operate stably. Some of these designs, for example, tilting pad bearings, achieve stability at the expense of steady state load capacity. One type of self-acting bearing that has good stability, and can also carry a higher load than a plain bearing, is the herringbone grooved bearing (refs. 1 to 3). Externally pressurized bearings also have a higher load capacity than plain self-acting bearings, and also are fairly stable (ref. 4).

The principal disadvantage of the externally pressurized bearing is the need for continuous supply of pressurized gas. The herringbone bearing, on the other hand, needs no external supply, but has no load capacity at zero speed. The two bearing types could be combined; for example, a herringbone grooved rotor could be installed in an externally pressurized bearing. External pressurization could be used for startup; upon reaching operating speed the external supply could be shut off, and the unit operated as a self-acting herringbone bearing. Alternately, the external supply could be maintained; the inward pumping of the herringbone grooves would reduce the amount of gas needed from the external supply.

Previous analyses have evaluated the load capacity and stability of herringbone grooved bearings (refs. 1 and 2) and of externally pres-

surized bearings (refs. 4 to 6). Vohr and Chow determined the load capacity of herringbone grooved bearings in reference 1; their analysis was used to evaluate stability in reference 2. Experimental stability data for herringbone bearings were obtained in reference 3. The data showed that the analysis predicts the onset of instability consistently; however, actual instability occurred at somewhat lower speeds than predicted.

The load capacity of externally pressurized bearings was determined by Lund in reference 5. In a later report (ref. 6), Lund calculated the stability of externally pressurized bearings operating at finite eccentricities. Here he included the effect of orifice recess volume, and attempted to account for having a finite number of orifices, rather than assuming a line source. Reference 4 evaluated the stability of an unloaded externally pressurized bearing, and included the effect of orifice recess volume as in reference 6.

All of these analyses are similar in that they use a small eccentricity perturbation, and solve for the perturbed pressure using a separation of variables scheme. Thus it is easy in principle to combine the solutions to find the load capacity and stability of a herringbone bearing with external pressurization.

The objectives of this investigation are to determine analytically the steady-state and stability characteristics of externally pressurized herringbone grooved bearings. Various combinations of supply pressure, feeding parameter, orifice recess volume, and groove length will be explored.

ANALYSIS

The analysis will be outlined briefly. More details are in reference 7. The bearing configuration to be analyzed is shown in figure 1. It consists of a double row externally pressurized bearing with herringbone grooves. The grooves are shown on the rotor, but the analysis is unchanged if they are on the bearing. The herringbone grooves may be partial, as shown, or they may extend the full length of the bearing. For simplicity of presentation, it will be assumed that the rows of orifices are closer to the midplane of the bearing than are the herringbone grooves. This includes the limiting case of the orifice rows coinciding with the ends of the grooves. Extension to other cases is straightforward. It will be further assumed that the bearing is symmetric about the midplane. With this assumption, only half the bearing need be analyzed. Other assumptions are that the number of herringbone grooves is large (ref. 1) and that there are enough orifices so that each row may be approximated by a line source.

The analysis of reference 1 applies, with the exception that the axial mass flow is no longer zero, as it was in the herringbone bearing without orifices. Thus, the differential equations and boundary conditions must be modified to account for axial mass flow in the bearing and flow through the orifices.

To conveniently obtain solutions for steady whirling, which are needed for the stability analysis, a rotating coordinate system is introduced by

$$\theta^* = \theta - \omega_p t \tag{1}$$

in which ω_p is the frequency of steady circular whirling. The differential equation to be solved, from reference 1, is

$$\frac{1}{R}\frac{\partial}{\partial\theta^*}\left[\dot{m}_{\theta r}\sin\beta + (\dot{m}_{zg} - \dot{m}_{zr})\alpha\cos\beta - \rho R\omega h_r\sin\beta\right] + \frac{\partial}{\partial z}\left[\alpha\dot{m}_{zg} + (1-\alpha)\dot{m}_{zr}\right]\sin\beta + (\omega - \omega_p)\frac{\partial}{\partial\theta^*}\left[\rho\alpha h_g - \rho(1-\alpha)h_r\right]\sin\beta = 0 \qquad (2)$$

This and subsequent expressions were derived for the herringbone grooved section of the bearing, but may also be used for the smooth section by setting $h_g = h_r$. The expressions for the mass flows $\dot{m}_{\theta r}$, $\dot{m}_{zg}$, and $\dot{m}_{zr}$ are in the appendix. The procedure now is to approximate the dimensionless film pressure $P = p/p_a$ according to

$$P(\theta^*, \zeta) \sim P_0(\zeta) + \epsilon\Re\omega\left[G(\zeta)e^{i\theta^*}\right] \qquad (3)$$

where ζ is the dimensionless axial coordinate z/L and G is a complex function of ζ. This is the classical small eccentricity perturbation solution originated by Ausman (ref. 8). Equation (3) and the expressions for mass flows from the appendix are substituted into equation (2). The resulting expression is considered an identity in the eccentricity ratio ϵ, and a separate equation written for each power of ϵ which appears. Powers of ϵ higher than 1 are neglected; thus, two equations result. The zero order equation can be written

$$\frac{d}{d\zeta}\left[\alpha\dot{m}_{zg0} + (1-\alpha)\dot{m}_{zr0}\right] = 0 \qquad (4)$$

This may be integrated once immediately to yield

$$\alpha\dot{m}_{zg0} + (1-\alpha)\dot{m}_{zr0} = \dot{m}_{z0} = \text{constant} \qquad (5)$$

In terms of the dimensionless pressure P_0, equation (5) for an isothermal bearing becomes

$$P_0\left[\mathcal{C}_p - \frac{dP_0}{d\zeta}\right] = \frac{12\mu\mathcal{R}T\mathcal{M}_{z0}R}{C^3P_a^2\mathcal{C}_1} = \text{constant} \tag{6}$$

The first order equation is

$$\frac{d^2G}{d\zeta^2} + \left[2\frac{dP_0}{d\zeta} - \mathcal{C}_p\right]\frac{dG}{d\zeta} + i\mathcal{C}_3P_0\frac{dG}{d\zeta}$$
$$+\left[\mathcal{C}_{4a}\frac{dP_0}{d\zeta} + \mathcal{C}_{4b}(\Lambda - \sigma) + \mathcal{C}_{4c}\right]iG - \mathcal{C}_5P_0G$$
$$-\left[\mathcal{C}_{6a}\frac{dP_0}{d\zeta} + \mathcal{C}_{6b}(\Lambda - \sigma) + \mathcal{C}_{6c}\right]iP_0 + \mathcal{C}_7\frac{dP_0}{d\zeta}$$
$$+\frac{1}{P_0}\left[\mathcal{C}_p - \frac{dP_0}{d\zeta}\right]\frac{dP_0}{d\zeta} = 0 \tag{7}$$

where the $\mathcal{C}$'s are constants given in the appendix. They differ from the constants given in reference 1 because $dP_0/d\zeta$ is not constant in a bearing with orifices. The constant Λ is the standard gas bearing compressibility number, and σ is a dimensionless representation of the whirl frequency.

Boundary conditions. - At the end of the bearing ($\zeta = 0$)

$$P = 1$$

and

$$G = 0 \tag{8}$$

At the bearing midplane ($\zeta = 1/2$), by symmetry.

$$\frac{dP_0}{d\zeta} = \frac{dG}{d\zeta} = 0 \tag{9}$$

Variables P_0 and G are continuous throughout the bearing film, but there will be discontinuities in the derivatives $dP_0/d\zeta$ and $dG/d\zeta$. These are caused at $\zeta = \zeta_g$ by the end of the herringbone groove pattern, and at $\zeta = \zeta_f$ by the gas flow through the orifices.

At the orifices, conditions are similar to those in an ungrooved externally pressurized bearing, analyzed in reference 5. One important difference is that in an externally pressurized herringbone bearing, the gas flow through the orifices can be in either direction, depending on the supply pressure and the pumping in the herringbone grooves. Boundary conditions on pressure are found by balancing the gas flow through the orifices with that through the bearing film. The results are

$$m_0 = - \frac{DP_{0c}}{L\Lambda_t} \left. \frac{dP_0}{d\zeta} \right|_{\zeta=\zeta_f^-} \tag{10}$$

and

$$\left. \frac{dG}{d\zeta} \right|_{\zeta=\zeta_f^+} = \left. \frac{dG}{d\zeta} \right|_{\zeta=\zeta_f^-} - \frac{L}{R} G_c \left[\frac{\psi_0}{P_s} + \frac{m_0 \Lambda_t}{2P_{0c}^2} + i\sigma\psi_1 \right] + \frac{1.5 + \delta^2}{1 + \delta^2} \frac{m_0 \Lambda_t L}{P_{0c} R} \tag{11}$$

in which ζ_f^+ denotes a value of ζ infinitesimally greater than ζ_f. The dimensionless gas flow m is given by the usual orifice flow equa-

tions, with inherent compensation effects accounted for as in reference 6.

$$m = \mathfrak{M}_z \frac{4R\sqrt{RT}\sqrt{1 + \left(\frac{\delta C}{h_r}\right)^2}}{Na^2 p_a} \tag{12}$$

$$m = \alpha_d P_s \sqrt{\frac{2k}{k+1}} \left(\frac{2}{k+1}\right)^{1/(k-1)} \qquad \frac{P_c}{P_s} \leq \left(\frac{2}{k+1}\right)^{k/(k-1)}$$

$$m = \alpha_d P_s \sqrt{\frac{2k}{k-1}} \left(\frac{P_c}{P_s}\right)^{1/k} \sqrt{1 - \left(\frac{P_c}{P_s}\right)^{(k-1)/k}} \qquad 1 \geq \frac{P_c}{P_s} > \left(\frac{2}{k+1}\right)^{k/(k-1)}$$

$$m = \alpha_d P_c \sqrt{\frac{2k}{k-1}} \left(\frac{P_s}{P_c}\right)^{1/k} \sqrt{1 - \left(\frac{P_s}{P_c}\right)^{(k-1)/k}} \qquad 1 > \frac{P_s}{P_c} > \left(\frac{2}{k+1}\right)^{k/(k-1)}$$

$$m = \alpha_d P_c \sqrt{\frac{2k}{k+1}} \left(\frac{2}{k+1}\right)^{1/(k-1)} \qquad \frac{P_s}{P_c} \leq \left(\frac{2}{k+1}\right)^{k/(k-1)}$$

(13)

The flow when the bearing is concentric, m_0, is obtained by using the concentric values $P_c = P_{0c}$ and $h_r = C$ in equations (12) and (13). The feeding parameter Λ_t appearing in equations (10) and (11) is defined by

$$\Lambda_t = \frac{6\mu Na^2\sqrt{RT}}{p_a C^3 \sqrt{1 + \delta^2}} \tag{14}$$

and ψ_1 in equation (11) by

$$\psi_1 = \frac{NV}{\pi DLC} \frac{L}{P_{0c}D} = \frac{vL}{P_{0c}D} \tag{15}$$

In differential equation (6) for P_0, $dP_0/d\zeta$ is the highest order derivative. Thus, the discontinuity in $dP_0/d\zeta$ at $\zeta = \zeta_g$ need not be found explicitly. The discontinuity in $dG/d\zeta$ at $\zeta = \zeta_g$ may be determined by noting that $\mathcal{m}_{z1} = \alpha \mathcal{m}_{zg1} + (1 - \alpha)\mathcal{m}_{zr1}$ is continuous at this point. The perturbed mass flows $\mathcal{m}_{zg1}$ and $\mathcal{m}_{zr1}$ may be found by differentiating the expressions for $\mathcal{m}_{zg}$ and $\mathcal{m}_{zr}$ with respect to ϵ and then setting $\epsilon = 0$, e.g.,

$$\mathcal{m}_{zg1} = \left.\frac{\partial \mathcal{m}_{zg}}{\partial \epsilon}\right|_{\epsilon=0}$$

The result for $dG/d\zeta$ is

$$\left.\frac{dG}{d\zeta}\right|_{\zeta=\zeta_g^+} = \frac{\Lambda_t m_0 L \mathcal{C}_m}{2P_0 R} + \mathcal{C}_1 \frac{L}{R}\left[\mathcal{C}_7 + \frac{1}{2} i \mathcal{C}_3 G\Big|_{\zeta=\zeta_g} + \left.\frac{dG}{d\zeta}\right|_{\zeta=\zeta_g^-}\right] \tag{16}$$

The expression for $\mathcal{C}_m$, as well as for the other $\mathcal{C}$'s, is in the appendix.

Solution of the differential equations. - The constant in equation (6) is determined by the gas flow through the orifices. From equation (12), with $\epsilon = 0$,

$$\mathcal{m}_{z0} = \frac{Na^2 p_a m_0}{4R\sqrt{RT}\sqrt{1 + \delta^2}} \tag{17}$$

Combination of equations (14) and (17) with equation (6) gives

$$\frac{dP_0}{d\zeta} - \mathcal{C}_p = -\frac{m_0 \Lambda_t}{2P_0 \mathcal{C}_1} \tag{18}$$

This differential equation contains two unknowns: the pressure P_0 and the mass flow m_0. The procedure for determining P_0 and m_0 is: (1) assume a value for m_0; (2) integrate equation (18) from $\zeta = 0$ to $\zeta = \zeta_f$, using a forward integration scheme such as Runge-Kutta (for $\zeta > \zeta_f$, $\mathcal{M}_{z0} = 0$ and $P_0 = P_{0c}$); (3) calculate a new value of m_0 from the value of $P_{0c} = P_0(\zeta_f)$ just found (eq. (13)); (4) compare with the previous m_0; if different, repeat steps 2-4 until convergence is obtained.

Differential equation (7) for G is solved numerically by the method detailed in reference 4.

Determination of load and stability. - The radial and tangential components of the bearing load are found by integrating the film pressure over the bearing area.

$$\begin{Bmatrix} F_r \\ F_t \end{Bmatrix} = \int_0^L \int_0^{2\pi} p_a P \begin{Bmatrix} -\cos\theta^* \\ \sin\theta^* \end{Bmatrix} R \, d\theta^* \, dz$$

Substitution of equation (3) for P and performance of the θ^* integration yields, in dimensionless variables,

$$\begin{Bmatrix} f_r \\ f_t \end{Bmatrix} = -\pi \begin{Bmatrix} Re \\ Im \end{Bmatrix} \int_0^{1/2} G \, d\zeta \tag{19}$$

The dimensionless forces in equation (19) are defined by

$$f_r = \frac{F_r}{\epsilon p_a LD}$$

and

$$f_t = \frac{F_t}{\epsilon p_a LD} \tag{20}$$

The resultant bearing load $\overline{W}$ and attitude φ may now be calculated.

$$\overline{W} = \frac{W}{\epsilon p_a LD} = \left(f_r^2 + f_t^2\right)^{1/2} \tag{21}$$

$$\varphi = \tan^{-1}\left(\frac{f_t}{f_r}\right) \tag{22}$$

Figure 2 illustrates the relations among these quantities.

When the bearing is operating stably, the frequency number σ is zero. To determine the threshold of instability, σ is varied until $f_t = 0$ (ref. 9). The bearing neutral stability condition is then found by equating the centrifugal force, due to the whirling bearing mass, to the radial bearing force.

$$Me\omega_{pn}^2 = F_{rn} \tag{23}$$

The subscript n denotes the condition where $f_t = 0$.

A dimensionless bearing mass may be defined by

$$\overline{M} = \frac{Mp_a}{2L\mu^2}\left(\frac{C}{R}\right)^5 \tag{24}$$

In terms of previously calculated quantities, $\overline{M}$ for the neutral stability condition is given by

$$\overline{M}_n = 144 \frac{f_{rn}}{\sigma} \tag{25}$$

Reference 9 shows that $\overline{M}_n$ is an upper limit of $\overline{M}$ for stability if the quantity $\partial f_t/\partial\sigma$ is negative at $\sigma = \sigma_n$; conversely, $\overline{M}_n$ is a lower limit for stability if $\partial f_t/\partial\sigma$ is positive at $\sigma = \sigma_n$.

RESULTS AND DISCUSSION

The analysis of the preceding section has been used to obtain steady state and stability information for a number of externally pressurized herringbone bearing configurations. Results were obtained utilizing the digital computer program presented in reference 7. The computer program was checked by running cases for a herringbone grooved bearing (without orifices) and a plain externally pressurized bearing (without grooves). Results for the test cases agreed well with those of references 1 and 4.

Because of the large number of parameters that may vary in a bearing, the effects of all of them were not investigated. Rather, a number of the parameters were fixed. The basic bearing chosen for study has a length to diameter ratio of 1 with a single row of orifices at the bearing midplane. No inherent compensation effects were included. The herringbone groove angle β is 30°, the groove width fraction α, 0.5, and the groove clearance to land clearance ratio, H, 2.1. The values approximate the optima found in reference 1 for maximizing the radial load component. Three groove length fractions were

investigated: 0 (ungrooved), 0.5, and 1 (fully grooved). The feeding parameter Λ_t was varied from 0 (no orifices) to 4, and the supply pressure ratio from 1 to 5.

Steady state results. - Figure 3 shows the effect of the feeding parameter Λ_t on load capacity. Figure 3(a) is for a pressure ratio P_s of 1, which means the bearing is actually unpressurized. For this case, the load capacity $\overline{W}$ is greatest when there are no orifices ($\Lambda_t = 0$); $\overline{W}$ decreases with increasing Λ_t. A partially grooved bearing will carry a higher load than a fully grooved bearing. The ungrooved bearing is not shown for this case, since it is unsuitable for most uses because it is unstable when not loaded.

Figure 3(b), for a pressure ratio of 2, shows that at low values of Λ (less than about 5) the load capacity now increases with increasing feeding parameter Λ_t. At higher Λ the order is reversed for the grooved bearings, that is, load capacity decreases with increasing Λ_t, as was the case for the unpressurized bearing. The partially grooved bearing's load capacity again exceeds that of the fully grooved bearing. For Λ less than 13 to 33 (depending on feeding parameter) the ungrooved bearing has the highest load capacity. At higher Λ, the load curves for the ungrooved bearings level off, while those for the grooved bearings continue to increase. This, of course, is because of the increasing self-pressurization by the inward pumping herringbone grooves.

The load curves for the grooved bearings show an interesting phenomenon in that they have a pronounced depression at an intermediate value of Λ. This depression occurs when the pumping of the herring-

bone grooves raises the pressure on the bearing side of the orifices to the pressure that is supplied externally. Near this point, the derivative of mass flow with respect to bearing orifice pressure P_c becomes very large (eq. (13)). That is, a very small change in P_c causes a large change in orifice flow. Consequently, the bearing is not as well "compensated" and the stiffness is reduced.

It should be pointed out that for an actual bearing the loss of the load capacity will not be as great as predicted by figure 3(b). This is because the difference $\Delta m/\Delta(P_c/P_s)$ for finite $\Delta(P_c/P_s)$ doesn't approach the infinite value of the derivative $\partial m/\partial(P_c/P_s)$. Also, the orifice flow equations (13) neglect viscous effects. These become significant at low flow rates, and would reduce the value of $\partial m/\partial(P_c/P_s)$ near $P_c = P_s$.

Load curves for a pressure ratio of 5 are plotted in figure 3(c). The trends of figures 3(a) and (b) are continued here. Load capacity increases with increasing Λ_t out to the highest compressibility number plotted. No depressions occur in the curves, as in figure 3(b), because the Λ value where $P_c = P_s$ is beyond the boundary of the figure.

Figures 3(b) and (c) show that the addition of grooves to an externally pressurized bearing lowers the load capacity at low compressibility numbers, but at higher Λ the load can be increased. The compressibility number where the grooved bearing's load capacity first becomes greater than that of the ungrooved bearing varies with the pressure ratio, length of grooves, and feeding parameter.

The effect of pressure ratio on load can be determined by comparing figures 3(a), (b), and (c). Load capacity generally increases with pressure ratio. The load capacity for $P_s = 2$ is little different than for $P_s = 1$ (unpressurized), particularly at higher compressibility numbers. Near the value of Λ where $P_c = P_s$ (depression in load curve) the load capacity for $P_s = 2$ can drop below that for $P_s = 1$. Increasing the pressure ratio to 5 results in a relatively large increase in load capacity, particularly at low compressibility numbers and large feeding parameters.

Attitude angles are plotted in figure 4 for a fully grooved bearing with a pressure ratio of 2. Except at quite low compressibility numbers ($\Lambda < 5$), attitude angles are smaller for smaller values of the feeding parameter Λ_t. The behavior is generally similar to an ungrooved externally pressurized bearing, with two exceptions. At zero speed ($\Lambda = 0$) the grooved bearing has a small negative attitude angle. In addition, when the pumping of the herringbone grooves increases the pressure P_c to near the supply pressure P_s, the attitude angle rises rapidly. This corresponds to the drop in load capacity mentioned earlier.

Because the herringbone grooves act as a pump, the gas flow through the bearing changes with compressibility number. Figure 5 shows the flow through the bearing, m_0, for 3 values of the feeding parameter Λ_t, at an external supply pressure ratio of 2.

For $\Lambda_t = 0$, the mass flow is always 0. A negative value of m_0 indicates the gas flow is from the pressurized supply to the bearing, while positive m_0 indicates the bearing is pumping gas into the pressurized supply. Flow doesn't change with compressibility number in the ungrooved bearings. To avoid confusion, these curves have not been extended to $\Lambda = 0$. At zero speed ($\Lambda = 0$), gas consumption increases with increasing length of grooves. This is because a grooved portion of a bearing has a larger flow area, and thus offers less resistance than an ungrooved portion.

Stability results. - In order to keep the figures presented to a reasonable number, stability information will not be given for all combinations of groove length, pressure ratio, feeding parameter, and orifice recess volume which were investigated. Instead, the basic bearing mentioned at the beginning of this section will be further defined, and results presented for variations of each of the preceding 4 parameters from their basic values. These basic values are $L_g/L = 1$, $P_s = 2$, $\Lambda_t = 2$, and $v = 0$.

Figure 6 shows the variation of stability with groove length for compressibility numbers from 1 to 50. Stability, as measured by the dimensionless mass $\overline{M}$, generally decreases with increasing Λ, and increases with groove length. Above a compressibility number of 15, the stability of the fully grooved bearing increases sharply, and becomes much greater than that of either the half-grooved or ungrooved bearing.

The stability curves of the fully-grooved and half-grooved bearings have distinct depressions near $\Lambda = 14$ and $\Lambda = 27$, respectively. These depressions correspond to the depressions in the load curves of figure 3(b). As was discussed regarding the load capacity curves, the drop in stability in an actual bearing whirling with a finite eccentricity would probably not be as drastic as figure 6 predicts. With an actual bearing, problems with this low stability region can probably be avoided by passing through the region rapidly, either by accelerating the bearing rotor or changing the supply pressure.

Near a compressibility number of 38, the stability curve for the half-grooved bearing becomes very steep, in effect imposing an upper speed limit even for very small values of $\overline{M}$. This limit generally occurred between compressibility numbers of 20 and 40 in the half-grooved bearings. A similar limit was not observed for fully grooved or ungrooved bearings within the range of compressibility numbers investigated.

The effect of the feeding parameter Λ_t on stability is shown by figure 7. At low compressibility numbers, ($\Lambda < 5$), higher feeding parameters give greater stability. Near $\Lambda = 14$, where the herringbone pumping pressure becomes equal to the supply pressure, the order is reversed, with the no-orifice bearing ($\Lambda_t = 0$) most stable. At high Λ (>20), there is no clear trend. The greatest stability is offered by $\Lambda_t = 2$, and the least by $\Lambda_t = 4$.

Figure 8 shows the effect on stability of a variation in supply pressure ratio. Included in this figure is the curve for $\Lambda_t = 0$; the remainder of the curves are for $\Lambda_t = 2$. For low compressibility numbers ($\Lambda < 10$), $P_s = 5$ provides the greatest stability; the curve is beyond the maximum ordinate of the figure. Stability decreases with decreasing pressure ratio. The plain herringbone bearing ($\Lambda_t = 0$) is between $P_s = 1$ and $P_s = 2$ ($P_s = 1$ denotes a bearing whose supply lines are open to the atmosphere). For compressibility numbers between 10 and 20 there is no clear optimum. At high Λ, pressure ratios of 1 and 2 are more stable than $P_s = 5$ or the no-orifice bearing. The figure shows that the addition of orifices to a herringbone bearing, without pressurization, lowers the stability at low compressibility numbers, but can increase the stability at high Λ.

The decrease in stability due to a small orifice recess is shown in figure 9. For compressibility numbers less than 14 there is only a small loss of stability. At higher Λ, however, the stability for a recess volume ratio of 0.2 continuously decreases, while the stability for $v = 0$ increases from $\Lambda = 14$ to $\Lambda = 40$. This behavior at higher compressibility numbers is typical of the effect of recess volume on the bearing configurations studied.

Multibranch curves. - For all cases of finite recess volume in grooved bearings, there was more than one neutral stability condition found at the higher compressibility numbers. That is, for a given Λ, there was more than one whirl frequency which yielded $f_t = 0$. Figure 10 illustrates this for a feeding parameter of 2, pressure ratio of 5,

and recess volume ratio of 0.2. The controlling curve will be the lowest; this will give the maximum value of $\overline{M}$ at which the bearing will be stable. Therefore, in using the analysis to determine stability, one must use some caution to be certain the smallest value of $\overline{M}_n$ has been found.

SUMMARY OF RESULTS

A small eccentricity analysis was performed to determine the steady state and stability characteristics of externally pressurized bearings with herringbone grooves. Compressibility numbers from 0 to 50 were investigated. The following results were obtained for a bearing with a single row of orifices and a length/diameter ratio of 1:

1. The addition of herringbone grooves to an externally pressurized bearing increases the bearing's stability. Grooving reduces load capacity at low compressibility numbers but increases load capacity at high compressibility numbers.

2. The fully grooved bearing is generally more stable than the partially grooved bearing. This is especially true at high compressibility numbers. However, the partially grooved bearing has a higher load capacity.

3. At low compressibility numbers, stability increases with increasing supply pressure and feeding parameter. At high compressibility numbers, there is no clear relation of stability with feeding parameter and supply pressure.

4. Load capacity and stability decrease, and the attitude angle increases near the speed where the pressure due to the herringbone groove pumping equals the external supply pressure. This is at least partly due to assumptions in the analysis.

5. Orifice recesses decrease stability. The effect is marked at high compressibility numbers. When there are orifice recesses, more than one neutral stability condition can exist at high compressibility numbers. The controlling condition is that which gives the lowest dimensionless mass for neutral stability.

APPENDIX - EXPRESSIONS FOR BEARING MASS FLOW AND DIFFERENTIAL EQUATION COEFFICIENTS

MASS FLOW EXPRESSIONS USED IN EQUATION (2) (FROM REF. 1)

$$\mathfrak{M}_{zg} = \frac{\rho}{12\mu} \frac{h_g^3}{\alpha h_r^3 + (1-\alpha)h_g^3} \left\{ (1-\alpha)\left(h_g^3 - h_r^3\right)\sin\beta\cos\beta \frac{1}{R}\frac{\partial p}{\partial \theta} + \left[h_r^3 + (1-\alpha)\left(h_g^3 - h_r^3\right)\sin^2\beta\right]\frac{\partial p}{\partial z} - 6\mu(1-\alpha)(U_p - U_g)(h_g - h_r)\sin\beta\cos\beta \right\}$$

$$\mathfrak{M}_{zr} = \frac{\rho}{12\mu} \frac{h_r^3}{\alpha h_r^3 + (1-\alpha)h_g^3} \left\{ -\alpha\left(h_g^3 - h_r^3\right)\sin\beta\cos\beta \frac{1}{R}\frac{\partial p}{\partial \theta} + \left[h_g^3 - \alpha\left(h_g^3 - h_r^3\right)\sin^2\beta\right]\frac{\partial p}{\partial z} + 6\mu\alpha(U_p - U_g)(h_g - h_r)\sin\beta\cos\beta \right\}$$

$$\mathfrak{M}_{\theta r} = -\frac{\rho}{12\mu} \frac{h_r^3}{\alpha h_r^3 + (1-\alpha)h_g^3} \left\{ \left[h_g^3 - \alpha\left(h_g^3 - h_r^3\right)\cos^2\beta\right]\frac{1}{R}\frac{\partial p}{\partial \theta} - \alpha\left(h_g^3 - h_r^3\right)\sin\beta\cos\beta\frac{\partial p}{\partial z} - 6\mu\alpha(U_p - U_g)(h_g - h_r)\sin^2\beta \right\} + \frac{\rho h_r}{2}(U_p + U_g)$$

DIFFERENTIAL EQUATION COEFFICIENTS

$$C_1 = \frac{H^3 + \alpha(1-\alpha)\left(H^3-1\right)^2 \sin^2\beta}{\alpha + (1-\alpha)H^3} \frac{R}{L}$$

$$C_p = \frac{\alpha(1-\alpha)(H^3-1)(H-1)\sin\beta\cos\beta\Lambda_s}{H^3 + \alpha(1-\alpha)\left(H^3-1\right)^2 \sin^2\beta}$$

$$C_3 = \frac{2\alpha(1-\alpha)\left(H^3-1\right)^2 \sin\beta\cos\beta}{H^3 + \alpha(1-\alpha)\left(H^3-1\right)^2 \sin^2\beta} \frac{L}{R}$$

$$C_{4a} = C_3$$

$$C_{4b} = -\frac{(\alpha H + 1 - \alpha)\left[\alpha + (1-\alpha)H^3\right]}{H^3 + \alpha(1-\alpha)\left(H^3-1\right)^2 \sin^2\beta} \left(\frac{L}{R}\right)^2$$

$$C_{4c} = \frac{\alpha(1-\alpha)(H^3-1)(H-1)\Lambda_s \sin^2\beta}{H^3 + \alpha(1-\alpha)\left(H^3-1\right)^2 \sin^2\beta} \frac{L}{R}$$

$$C_5 = \frac{H^3 + \alpha(1-\alpha)\left(H^3-1\right)^2 \cos^2\beta}{H^3 + \alpha(1-\alpha)\left(H^3-1\right)^2 \sin^2\beta} \left(\frac{L}{R}\right)^2$$

$$C_{6a} = \frac{3\alpha(1-\alpha)(H^3-1)(H-1)\sin\beta\cos\beta\left[\alpha(H^2-H-1) - (1-\alpha)H^2(H^2+H-1)\right]}{\left[H^3 + \alpha(1-\alpha)\left(H^3-1\right)^2 \sin^2\beta\right]\left[\alpha + (1-\alpha)H^3\right]} \frac{L}{R}$$

$$C_{6b} = \frac{\alpha + (1-\alpha)H^3}{H^3 + \alpha(1-\alpha)\left(H^3-1\right)^2 \sin^2\beta} \left(\frac{L}{R}\right)^2$$

$$\mathcal{C}_{6c} = \frac{3\alpha(1-\alpha)(H-1)^2 H^2 \Lambda_s \sin^2\beta}{\left[H^3 + \alpha(1-\alpha)\left(H^3-1\right)^2 \sin^2\beta\right]\left[\alpha + (1-\alpha)H^3\right]} \frac{L}{R}$$

$$\mathcal{C}_7 = \frac{3\alpha(1-\alpha)(H-1)(H^2-1)\Lambda_s \sin\beta\cos\beta\left[H^2(H^2+1) + \alpha(1-\alpha)\left(H^3-1\right)^2 \sin^2\beta\right]}{\left[H^3 + \alpha(1-\alpha)\left(H^3-1\right)^2 \sin^2\beta\right]^2}$$

$$\mathcal{C}_m = \frac{3\alpha H^2(H-1)\left[1 + (1-\alpha)(H^3-1)\left(2 + (1-\alpha)(H^3-1)\right)\sin^2\beta\right]}{\left[H^3 + \alpha(1-\alpha)\left(H^3-1\right)^2 \sin^2\beta\right]^2}$$

In the ungrooved portion of the bearing, these coefficients become:

$$\mathcal{C}_1 = \frac{R}{L}$$

$$\mathcal{C}_p = 0$$

$$\mathcal{C}_3 = 0$$

$$\mathcal{C}_{4a} = 0$$

$$\mathcal{C}_{4b} = -\left(\frac{L}{R}\right)^2$$

$$\mathcal{C}_{4c} = 0$$

$$\mathcal{C}_5 = \left(\frac{L}{R}\right)^2$$

$$\mathcal{C}_{6a} = 0$$

$$\mathcal{C}_{6b} = \left(\frac{L}{R}\right)^2$$

$$\mathcal{C}_{6c} = 0$$

$$\mathcal{C}_7 = 0$$

REFERENCES

1. Vohr, J. H., and Chow, C. Y., "Characteristics of Herringbone-Grooved, Gas-Lubricated Journal Bearings," J. Basic Eng. vol. 87, 1965, pp. 568-578.

2. Reiger, N. F., ed., Design of Gas Bearings. Vol. 1: Design Notes, Mechanical Technology, Inc., 1966.

3. Cunningham, R. E., Fleming, D. P., and Anderson, W. J., "Experimental Stability Studies of the Herringbone-Grooved Gas-Lubricated Journal Bearing," J. Lubr. Tech., vol. 91, 1969, pp. 52-59.

4. Fleming, D. P., Cunningham, R. E., and Anderson, W. J., "Zero-Load Stability of Rotating Externally Pressurized Gas-Lubricated Journal Bearings," ASME Paper 69-Lub-27, 1969, to be published in Journal of Lubrication Technology.

5. Lund, J. W., "The Hydrostatic Gas Journal Bearing with Journal Rotation and Vibration," J. Basic. Eng., vol. 86, 1964, pp. 328-336.

6. Lund, J. W., "A Theoretical Analysis of Whirl Instability and Pneumatic Hammer for a Rigid Rotor in Pressurized Gas Journal Bearings," J. Lubr. Tech., vol. 89, 1967, pp. 154-166.

7. Fleming, D. P., "Steady-State and Stability Analysis of Externally Pressurized Gas-Lubricated Journal Bearings with Herringbone Grooves," proposed NASA Technical Note.

8. Ausman, J. S., "Finite Gas-Lubricated Journal Bearing," Proceedings of the Conference on Lubrication and Wear, Inst. Mech. Eng., 1957, pp. 39-45.

9. Pan, C. H. T., "Spectral Analysis of Gas Bearing Systems for Stability Studies," Dynamics and Fluid Mechanics, Vol. 3, Part 2 of Developments in Mechanics, T. C. Huang and M. W. Johnson, Jr., eds., John Wiley & Sons, Inc., New York, 1965, pp. 431-447.

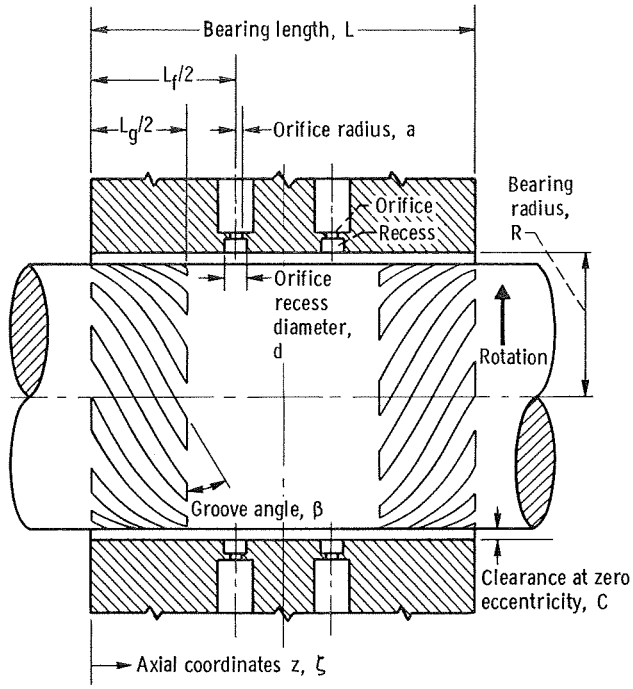

Figure 1. - Externally pressurized herringbone bearing.

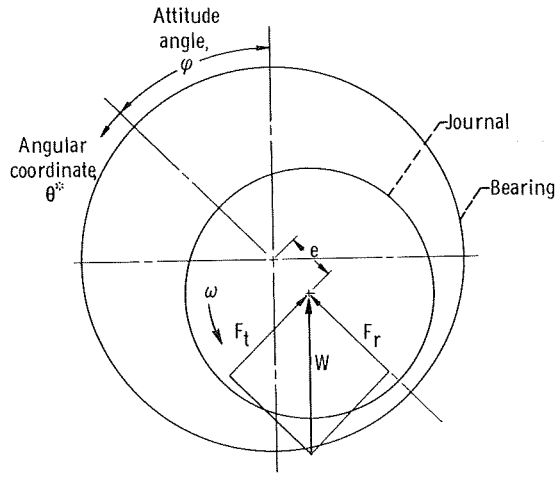

Figure 2. - Notation for eccentric bearing.

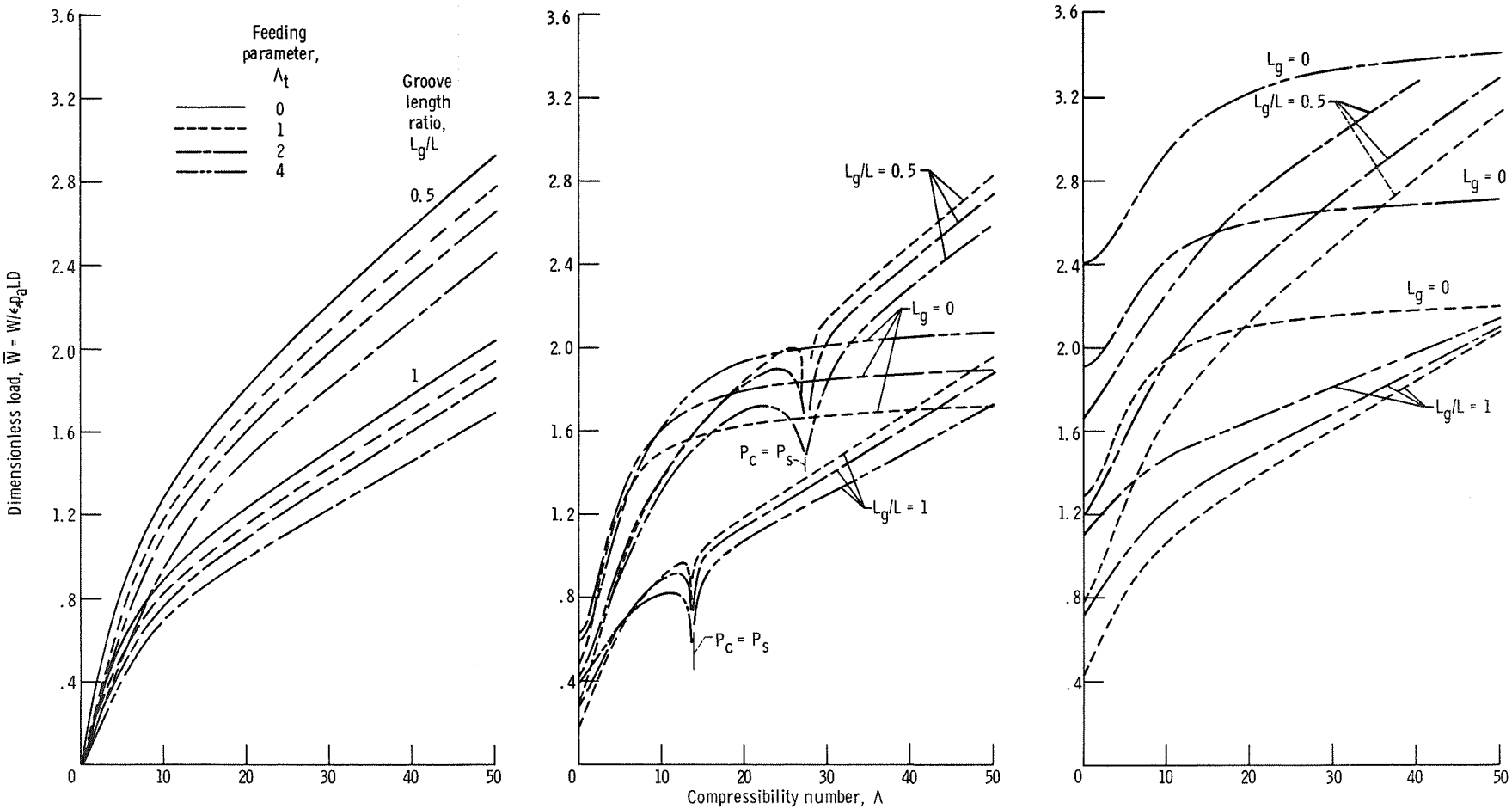

(a) Pressure ratio P_s, 1.

(b) Pressure ratio P_s, 2.

(c) Pressure ratio P_s, 5

Figure 3. - Effect of feeding parameter Λ_t on load. L/D = 1, L_f/L = 1, β = 30°, α = 0.5, H = 2.1.

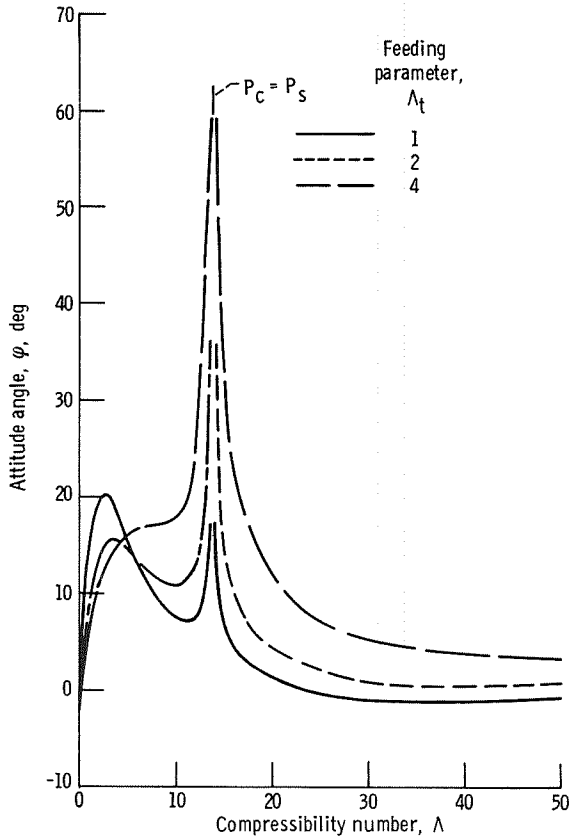

Figure 4. - Effect of feeding parameter on attitude angle. $L_g/L = 1$, $P_s = 2$, $L/D = 1$, $L_f/L = 1$, $\beta = 30°$, $\alpha = 0.5$, $H = 2.1$.

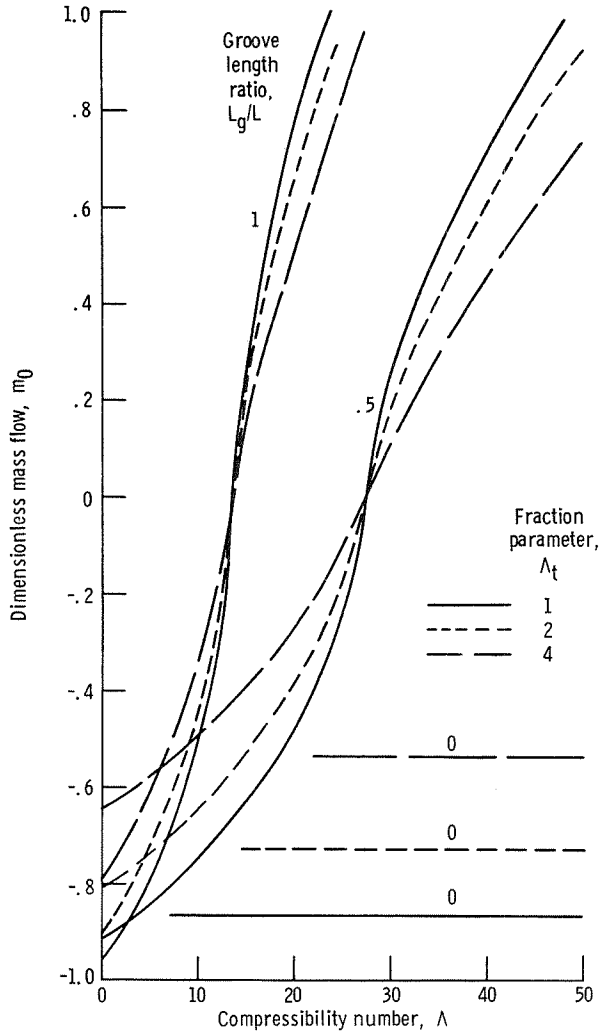

Figure 5. - Gas flow through bearing. $P_s = 2$, $L/D = 1$, $L_f/L = 1$, $\beta = 30°$, $\alpha = 0.5$, $H = 2.1$.

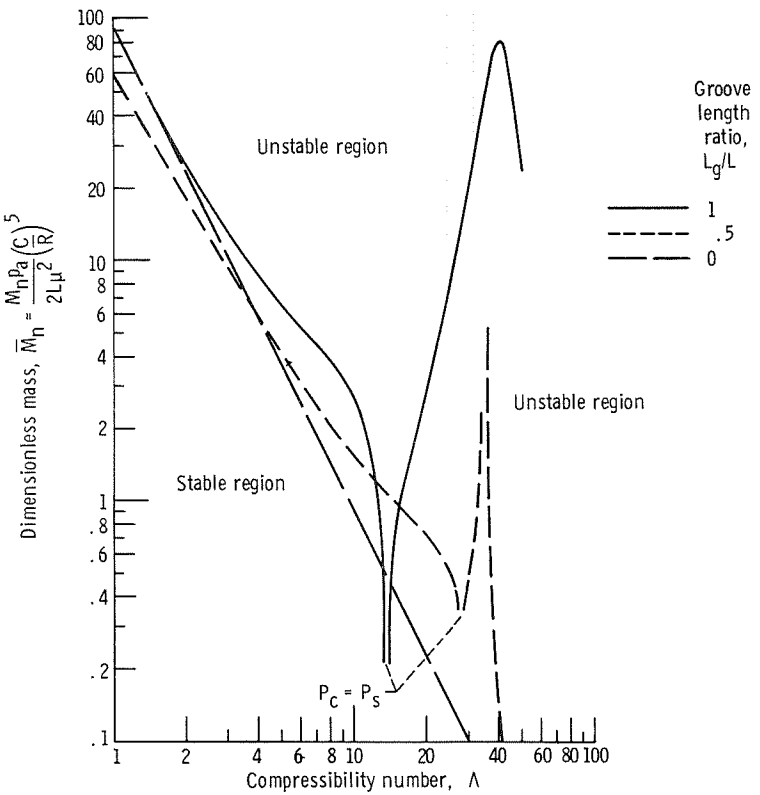

Figure 6. - Effect of groove length on stability. $P_s = 2$, $\Lambda_t = 2$, $v = 0$, $L/D = 1$, $L_f/L = 1$, $\beta = 30°$, $\alpha = 0.5$, $H = 2.1$.

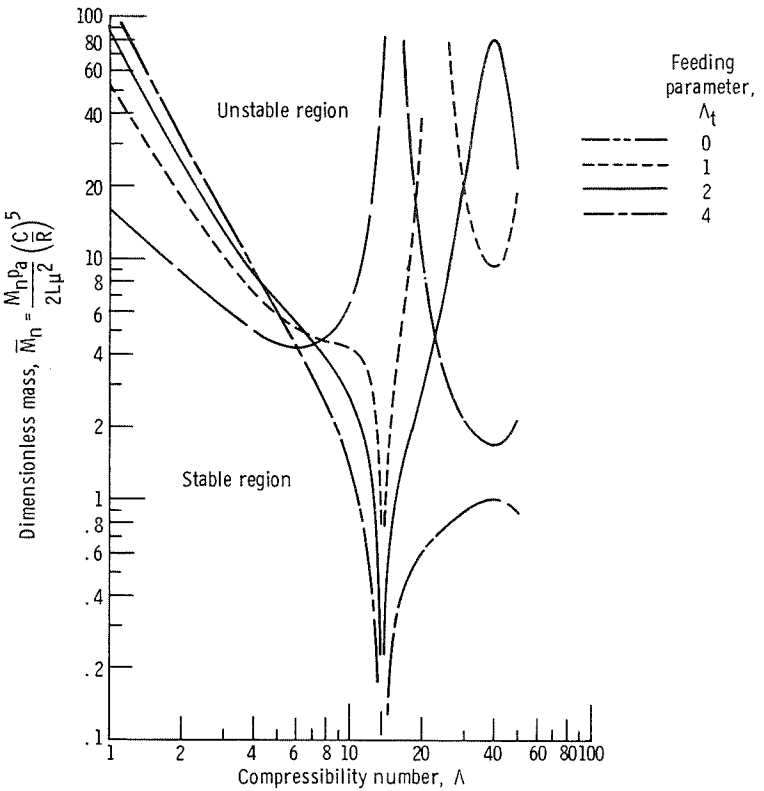

Figure 7. - Effect of feeding parameter on stability. $P_s = 2$, $L_g/L = 1$, $v = 0$, $L/D = 1$, $L_f/L = 1$, $\beta = 30°$, $\alpha = 0.5$, $H = 2.1$.

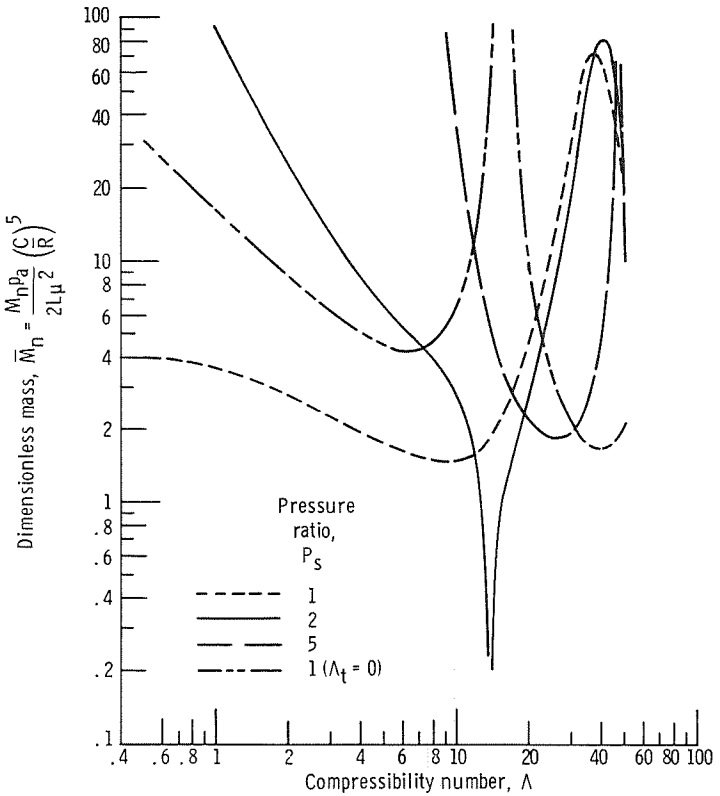

Figure 8. - Effect of pressure ratio on stability. $\Lambda_t = 2$, $L_g/L = 1$, $v = 0$, $L/D = 1$, $L_f/L = 1$, $\beta = 30°$, $\alpha = 0.5$, $H = 2.1$.

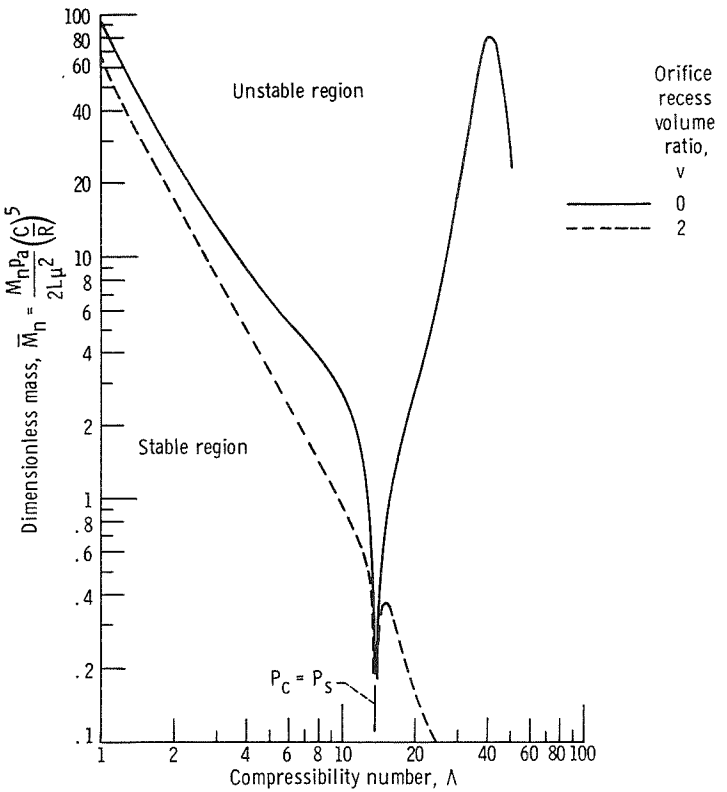

Figure 9. - Effect of recess volume on stability. $P_s = 2$, $\Lambda_t = 2$, $L_g/L = 1$, $\beta = 30°$, $\alpha = 0.5$, $H = 2.1$.

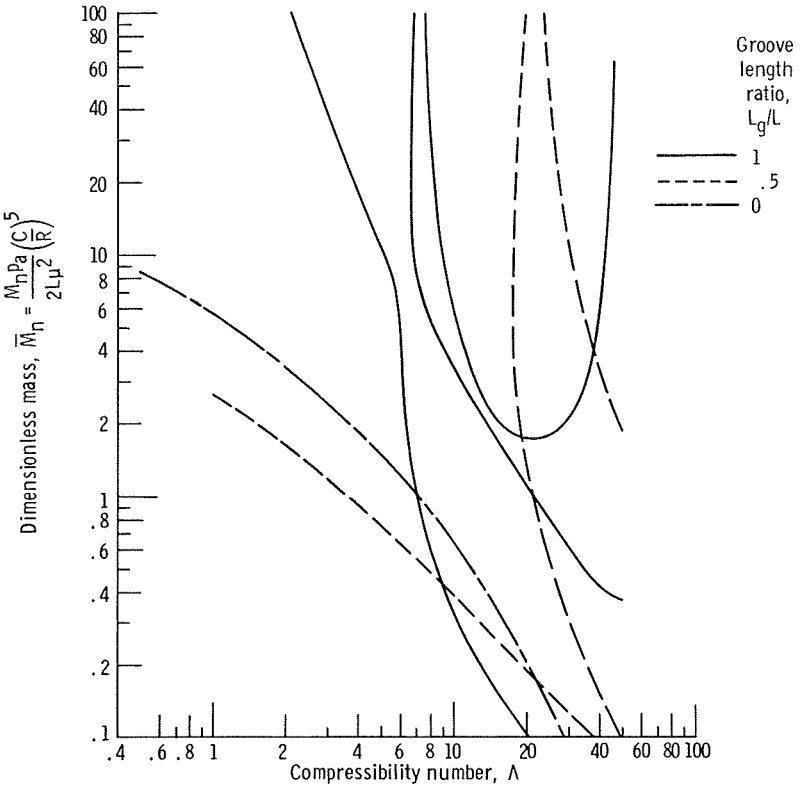

Figure 10. - Multi-branch curves. $v = 0.2$, $P_s = 5$, $\Lambda_t = 2$, $L/D = 1$, $L_f/L = 1$, $\beta = 30°$, $\alpha = 0.5$, $H = 2.1$.